VENTED HYDROGEN DEFLAGATIONS IN AN ISO CONTAINER

Vendra C. Madhav Rao[1] and Jennifer X. Wen[2]
[1] Warwick FIRE, School of Engineering, University of Warwick, Coventry CV4 7AL, UK
[2] Warwick FIRE, School of Engineering, University of Warwick, Coventry CV4 7AL, UK,

Correspondence: Jennifer.wen@warwick.ac.uk

ABSTRACT

The commercial deployment of hydrogen will often involve housing portable hydrogen fuel cell power units in 20-foot or 40-foot shipping containers. Due to the unique properties of hydrogen, hazards identification and consequence analysis is essential to safe guard the installations and design measures to mitigate potential hazards. In the present study, the explosion of a premixed hydrogen-air cloud enclosed in a 20-foot container of 20' x 8' x 8'.6" is investigated in detail numerically. Numerical simulations have been performed using HyFOAM, a dedicated solver for vented hydrogen explosions developed in-house within the frame of the open source computational fluid dynamics (CFD) code OpenFOAM toolbox. The flame wrinkling combustion model is used for modelling turbulent deflagrations. Additional sub-models have been added to account for lean combustion properties of hydrogen-air mixtures. The predictions are validated against the recent experiments carried out by Gexcon as part of the HySEA project supported by the Fuel Cells and Hydrogen 2 Joint Undertaking (FCH 2 JU) under the Horizon 2020 Framework Programme for Research and Innovation. The effects of congestion within the containers on the generated overpressures are also investigated.

Keywords: Vented explosion, Hydrogen, OpenFOAM, Flame Wrinkling Model, 20-ft ISO container

1.0 INTRODUCTION

Venting process is widely used for mitigating the damage to the process equipment and the enclosure in case of an accidental gas explosion. Suitable venting area and location must be provided to ensure that the overpressure is released sufficiently faster than the rate of pressure generation by the combustion process in the enclosure. Hydrogen is widely considered suitable future energy carrier to address both the climate change problem and to handle the scenario of depleting resources for the fossil fuels. The usage of hydrogen fuel cells is on increase in automotive sector and in portable power generation units. The commercial deployment of hydrogen will often involve housing portable hydrogen fuel cell power units in 20-foot or 40-foot shipping containers. Due to the unique properties of hydrogen, hazards identification and consequence analysis is essential to safe guard the installations and design measures to mitigate potential hazards.

To understand the factors that effects vented explosion process, many experimental and numerical studies have been performed in the last few decades [1-5]. The venting of lean hydrogen mixtures is studied to further access the influence of the hydrogen gas properties in the venting process [5-8]. The Lewis number effects are important in the lean hydrogen-air combustion processes [9-10]. Hence suitable modelling correction should be done to take into account the Lewis number effects into turbulent flame deflagration modelling. Flame instabilities are also found to have dominating effects on the venting process of the lean hydrogen mixtures [5-6]. The Darrieus–Landau and thermodiffusive instabilities also affects the flame propagation in lean hydrogen mixtures. While venting of hot gases occurs through vent areas, Helmholtz oscillations are generated within the vessel due to expulsion of bulk of the gas and the resulting flame accelerations give rise to Rayleigh-Taylor instabilities of the flame front. These instabilities are studied in numerical modelling either using an algebraic expression or solving a transport equation [5-6]. The various factor mentioned above present in the turbulent lean hydrogen deflagrations but they influence are dominant at different stages of the flame development. The Darrieus–Landau and thermodiffusive instabilities are found to be dominant in the initial stage of flame propagation after the start of the ignition process. The Helmholtz oscillations and Rayleigh-

Taylor instabilities tend to contribute in the later stage venting process, when the hot gases start to exit from the vent area.
Recently some of the experiments for full scale ISO container configuration have been carried out by Gexcon as part of the HySEA project supported by the Fuel Cells and Hydrogen 2 Joint Undertaking (FCH 2 JU) under the Horizon 2020 Framework Programme for Research and Innovation. In the present study, numerical modelling and simulations are being conducted to further aid our understanding of the vented gas explosion in these self-contained portable power units using the opensource Computational Fluid Dynamics (CFD) code OpenFOAM.[10] solver HyFOAM.

2.0 NUMERICAL MODELLING

HyFOAM has been developed in-house within the frame of open source Computational Fluid Dynamics (CFD) code OpenFOAM tool box [11] for vented lean hydrogen explosions. The governing Navier-Stokes equations are solved using the Large Eddy Simulation (LES) approach with a collocated, finite-volume method, a fully compressible Pressure-Implicit Split Operator (PISO) solution method. Diffusion terms are discretized using a second-order accurate central differencing scheme and the advective terms approximated using a second-order accurate limited linear scheme. The transient term was discretized using a fully implicit, second-order accurate three-time-level method [11]. A one equation eddy viscosity model is used for evaluating the subgrid scale (SGS) turbulence [12]. The main difficulty in LES is the proper treatment of the flame front or the reaction zone, since the characteristic scales for turbulent combustion are in the SGS, for which SGS reaction rate models are required. The Flame Surface Wrinkling Model developed by [13] is adopted for simulating the turbulent deflagrations. The set of governing equations are solved sequentially with iteration over the explicit coupling terms to obtain convergence. The segregate approach results in a Courant number restriction[13]. Courant number of 0.1 was used in the present numerical simulations. The following section deals with the description of the Flame Surface Wrinkling Model completing the governing equation for the reacting flows.

2.1 Combustion model

The flamelet concept simplifies the turbulent combustion treatment by separating the combustion modelling from the analysis of the turbulent flow field by assuming that reaction takes place in relatively thin layers that separate regions of unburned and fully burned gases. The laminar flamelet approach is used with conditional filtering to create a set of transport equations representing the complex combustion process [13, 14]. The unburnt zone volume fraction is denoted as regress variable (b), taking values b = 1 in fresh gases and b = 0 in fully burnt gas region. The transport equation for the resolved part of regress variable (b) is given as:

$$\frac{\partial \overline{\rho}\tilde{b}}{\partial t} + \nabla.\left(\overline{\rho}\tilde{U}\tilde{b}\right) - \nabla.\left(\overline{\rho}\mu_{sgs}\nabla\tilde{b}\right) = -\overline{\rho_u} S_L \Xi \left|\nabla\tilde{b}\right| \tag{1}$$

where, Ξ is subgrid flame wrinkling, can be regarded as the turbulent to laminar flame speed ratio and is formally related to the flame surface density by $\sum = \Xi |\nabla \overline{b}|$, ρ is the density, S_L is laminar flame speed and μ_{sgs} is the subgrid turbulent diffusion coefficient. Symbols ($\overline{\ }$) and ($\tilde{\ }$) represent the filtered and the density weighted filtering operations respectively. The subscripts u indicates conditioning on the unburned gases region. The resolved unburned gas volume fraction $\overline{b}$ is related to $\tilde{b}$ through $\overline{\rho}_u \overline{b} = \overline{\rho}\tilde{b}$. The closure for the sub-grid wrinkling is provided by a balanced transport equation,

$$\frac{\partial \overline{\rho}\Xi}{\partial t} + \hat{U}_s.\nabla\Xi = \overline{\rho} G \Xi - \overline{\rho} R(\Xi - 1) + \overline{\rho}\max\left[\left(\sigma_s - \sigma_t\right), 0\right]\Xi \tag{2}$$

where, U_s is the surface filtered local instantaneous velocity of the flame, which is modelled as

$$\tilde{U}_s = \tilde{U} + (\frac{\bar{\rho}_u}{\bar{\rho}} - 1) S_L \Xi n_f - \frac{\nabla.(\bar{\rho}\,\mu_{sgs} \nabla \tilde{b})}{\bar{\rho}\,|\nabla \tilde{b}|} n_f \tag{3}$$

The direction of flame propagation is $n_f = \nabla\tilde{b} / |\nabla\tilde{b}|$, σ_S and σ_t are the surface filtered resolved strain-rates relating to the surface filtered local instantaneous velocity of the flame (U_s) and surface filtered effective flame velocity of the flame surface (U_t), modelled as

$$\sigma_t = \nabla.(\tilde{U} + S_L \Xi\, n_f) - n_f.[\nabla(\tilde{U} + S_L \Xi n_f)].n_f$$

$$\sigma_s = \frac{\nabla.\tilde{U} - n_f.(\nabla\tilde{U}).n_f}{\Xi} + \frac{(\Xi+1)[\nabla.(S_L n_f) - n_f.[\nabla(S_L n_f).n_f]}{2\Xi} \tag{4}$$

The terms $G\Xi$ and $R(\Xi - 1)$ in equation 2 are sub-grid turbulence generation and removal rate, with G and R as rate coefficients requiring modelling. The modelling of these terms is based on flame-speed correlation of [14] are given below

$$G = R\frac{\Xi_{eq} - 1}{\Xi_{eq}} \quad \text{and} \quad R = \frac{0.28}{\tau_\eta}\frac{\Xi^*_{eq}}{\Xi^*_{eq} - 1},$$

$$\Xi^*_{eq} = 1 + \frac{0.46}{Le} Re_t^{0.25} \left(\frac{\hat{u}}{S_{Lo}}\right)^{0.3} \text{and } \Xi_{eq} = 1 + 2(1-b)(\Xi^*_{eq} - 1) \tag{5}$$

where, τ_n is the Kolmogorov time scale, $\hat{u}$ is the sub grid turbulence intensity and Re_t is the turbulent Reynolds number. The modelling of the terms in equation (5) for lean turbulent premixed combustion takes into account the Lewis number (Le) effects in the turbulent flame speed correlation The algebraic reaction rate closure, MFSD proposed in [15] is adopted in the present study. This model has been successfully applied to both pure and mixed fuels, under varying Lewis number conditions [10] [16] [17], in both RANS and LES contexts. The MFSD model predictions for the turbulent flame speed (S_T) for equivalence ratio between and inclusive of 0.4 and 0.8 along with Goulier's [18] correlation is compared with the available experimental measured values of [19]. These results are shown in figure 1. The Muppala models (MFSD) analytical predictions of S_T trends are consistent for the turbulence levels quantitatively to the experimental results in consideration.

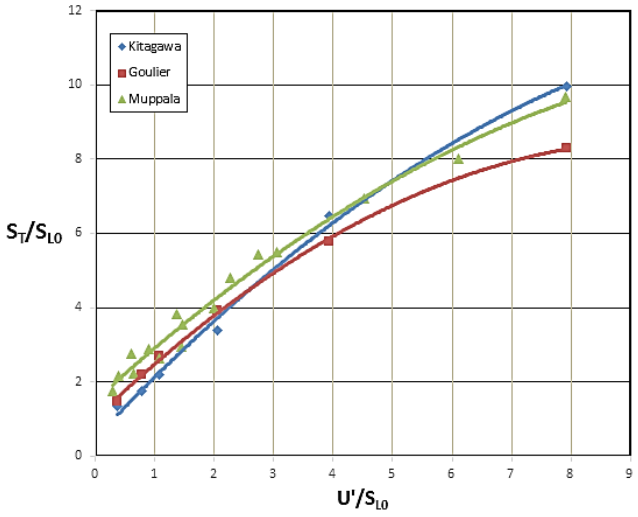

Figure 1. Comparison of turbulent flame speed correlation of [18] [15] with the experimental data of [19].

The Darrieus–Landau and thermodiffusive instabilities also affects the flame propagation in lean mixtures. These instabilities are modelled considering the analytical expression proposed by [7]. The flame wrinkling due to the Darreius-landau instabilities is modelled as algebraic expression based on [7] as,

$$\Xi_{DL} = \max\left[1, \alpha_1 \left(\frac{\Delta}{\lambda_c}\right)^{1/3}\right] \tag{6}$$

where, λ_c is cutoff wavelength of unstable scales and $\propto_1$ is a coefficient to account for uncertainty in λ_1. The unstrained laminar flame speed ($S_{L,0}$) for lean hydrogen-air mixture is adopted based on the numerical study carried out by [20], for evaluating S_L at a given equivalence ratio ($\phi = 1/\lambda$) and reference condition, expressed as power law function of elevated temperature and pressure,

$$S_L = S_{L0}(\lambda, P)\left(\frac{T_u}{T_{uo}}\right)^{\propto(\lambda,\ P)} \tag{7}$$

$$S_{L0} = 499.63 - 308.60\lambda + 48.887\lambda^2 - 76.238P + 4.825P^2 + 45.813\lambda P - 2.926\lambda P^2 - 7.163\lambda^2 P + 0.436\lambda^2 P^2$$

$$\alpha(\lambda, P) = 1.85175 - 0.70875\lambda + 0.50171\lambda^2 - 0.19366P + 0.0067834P^2 + 0.27495\lambda P - 0.0088924\lambda P^2 - 0.052058\lambda^2 P + 0.00146015\lambda^2 P^2$$

where S_L in cm/s , P is pressure in bar and T_u unburnt gas temperature in K. The above correlation is valid for the equivalence ratios (ϕ) between 0.33 and 0.47 (lean mixtures), pressures range of 1bar $\leq$ P $\leq$ 8.5 bar and temperature range of 300 K $\leq$ T $\leq$ 800 K, with reference state Tu_0 = 300 K. The flame wrinkling factor is equation (1) is evaluated as

$$\Xi = \Xi_t * \Xi_{DL} \tag{8}$$

Thus, equations (1)-(8) complete the combustion model description for lean hydrogen mixtures in HyFOAM solver.

3.0 EXPERIMENTS CONSIDERED

The typical 20-ft ISO container of dimensions 20'x 8'x 8'.6" used in the experiments is been shown in Figure 2. Test data from full scale container tests carried out by Gexcon (submitted separately for this conference) are used for model validation.

Figure 2. A typical standard 20 ft. ISO container used in the experiments [21].

The walls of the container are corrugated and 2 mm in thickness. The dimensions of the container at the outside are 6.058 m × 2.591m × 2.438 m and inside are 5.867m × 2.385 m × 2.352 m. The homogenous gas mixture inside the container for a given volumetric composition was prepared using recirculation method. The container doors having dimensions 2.225 m high, 1.114 m wide and 50 mm thick were kept open in perpendicular position to the container (See Figure 5(a)). The front section of the container is covered with polyethylene sheet to retain the combustible gas mixture. The container was positioned 0.36 m above ground level on H-beams shown in figure 3 (b) lower part. The instrumentation and obstacle holding steel frame is fixed to the floor of the container. The frame is constructed using U-beams (200 mm X 75 mm) steel sections, shown in Figure 3(b). The two model obstacles, 1) 20 gas bottles held in a basket and 2) pipe rack, both representative of the congestion present in a power generation unit are used in the experiments. The individual gas bottles in the bottles basket obstacle are of 50-litre steel cylinders, with diameter 0.23 mm and height 1.66 m from the floor to the top of the valve. The cylinders are mounted in a basket made from 50 mm × 50 mm square steel pipe and spacers fix the gaps between the bottles to about 5 mm. The overall external dimensions of the bottle basket are about 1.27 m × 1.04 m as shown in Figure 3 (c).

(a) Wall corrugation

(b) Steel frame (top part)

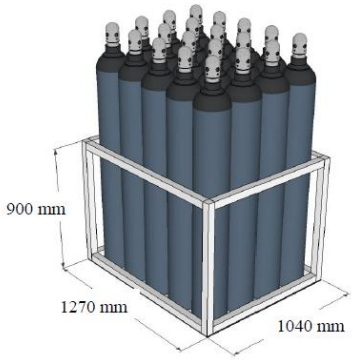

(c) Bottle basket

(d) Pipe rack

Figure 3. Congestion and constrictions with in the containers [21].

The pipe rack obstacle configuration consists of a frame made by 0.1 m × 0.1 m square steel pipes with outer dimensions 2.0 m high, 1.3 m long, and 1.1 m wide. This obstacle includes four layers of pipes laid laterally as shown in figure (d), the two layers with five 104 mm diameter pipes and two double layers with 2 × 11 pipes with diameter 20 mm. Within the container the pressure sensors are place symmetrically on the steel frame at distance 0.86 m (P1-P2), 2.45 m (P3-P4), 4.0 m (P5-P5) and 5.56 m (P7-P8) from the backend container wall with 0.2 m elevation from the container floor. Outside the open doors of the container, the pressure probes are placed at an elevation of 1.65 m and at 5 m (P9), 10 m (P10) and 15 m (P11) distance from the open-end along the centreline, as shown in Figure 4.

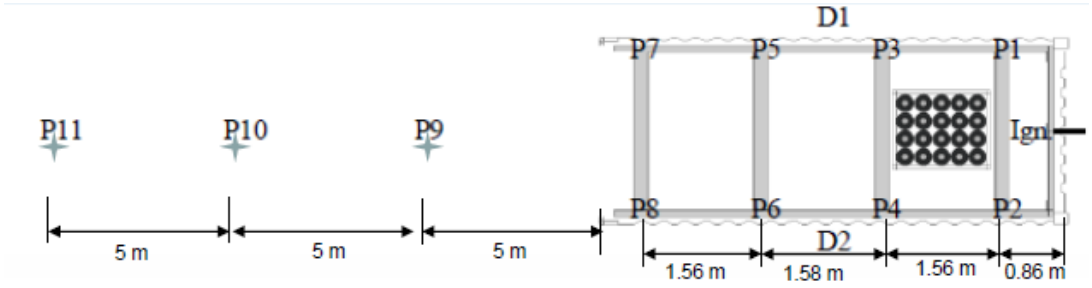

Figure 4. Overpressure monitoring points with respect to the frame and container [21].

The pressure sensor was fitted on to a plate fixed at the top of the vertical tube, about 1.65 m above ground, measuring the side-on pressure. D1 and D2 are two laser probes placed on either side of the container to measure the container deflections with regard to time from start of ignition. The ignition of the homogenous mixture is done using an electric inductive spark located at the back wall of the container, along the centreline, and at mid height.

4.0 NUMERICAL SETUP

The standard 20-ft ISO container details used in the numerical simulation are shown in Figure 5. The series of experiments were conducted by the Gexcon under varying conditions of hydrogen concentration from 15% - 21% by volume, with or without any obstacles inside the container. To validate the numerical modelling in the present study, three scenarios experimental (case studies) are considered:

1) Case-1: simple configuration of no obstacles, steel frame inside the container and doors fully open with 15 % hydrogen concentration by volume as shown in Figure 5(b).

2) Case-2: configuration with bottle basket inside the container close to the back end and doors fully open with 15 % hydrogen concentration by volume as shown in Figure 6(a).

3) Case-3: configuration of pipe rack inside the container close to the backend and doors fully open with 15 % hydrogen concentration by volume as shown in Figure 6(b).

The ignition of the hydrogen mixture was initiated by creating a spherical hot patch at the centre of the back end wall at the mid height of the container with products composition and temperature, mimicking the electric inductive spark used in the experiments. The numerical computational domain with the obstacles inside the container are shown in Figure 6.

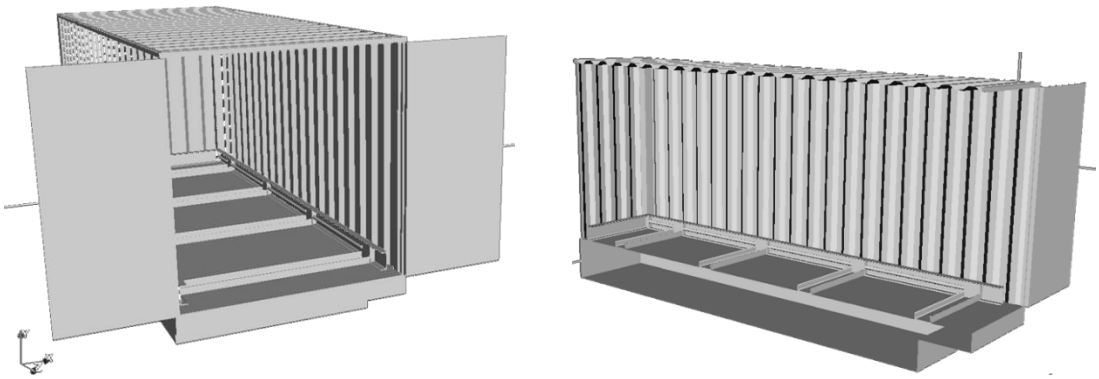

(a) Isometric view (b) Cut section along the centreline

Figure 5. The standard 20-ft ISO container with frame to hold the pressure sensors in the experiments.

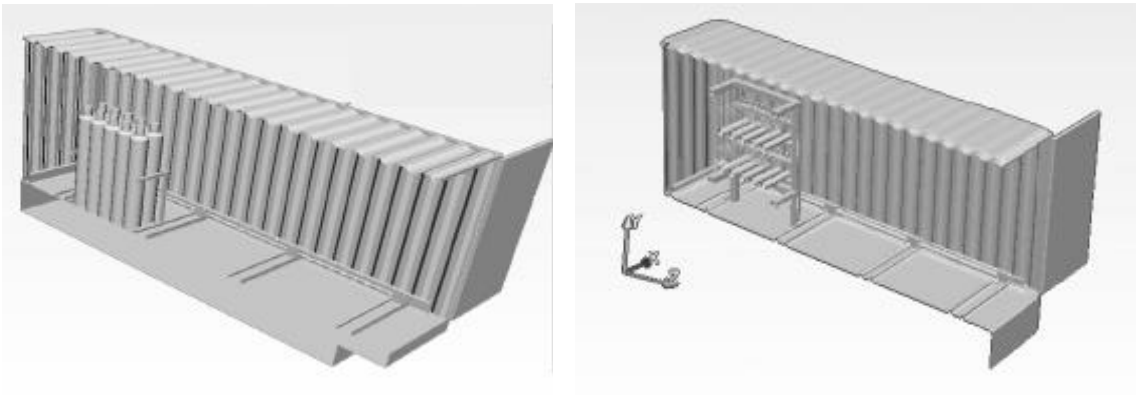

(a) With bottle basket obstacle (b) With pipe rack obstacle

Figure 6. The standard 20-ft ISO container with model obstacles.

An hybrid hexagon-tetrahedral computational mesh was generated for the container geometry using the 'SnappyHexMesh' utility in OpenFOAM. The mesh distribution in the computation domain is shown in Figure 7. The volume enclosing the container, 30.0 m × 15.0 m × 35 m was also meshed to capture the venting of the burnt gas, the external explosions and to reduce the effect of boundary conditions on the numerical results. A non-uniform cell size of 0.5 cm was used in the ignition region, a 3 cm cell size inside the chamber and in the area immediately outside the chamber to resolve the external explosion. The total cells in computational mesh are approximately between 3.5 ~ 4.6 million for the three cases considered in the present study.

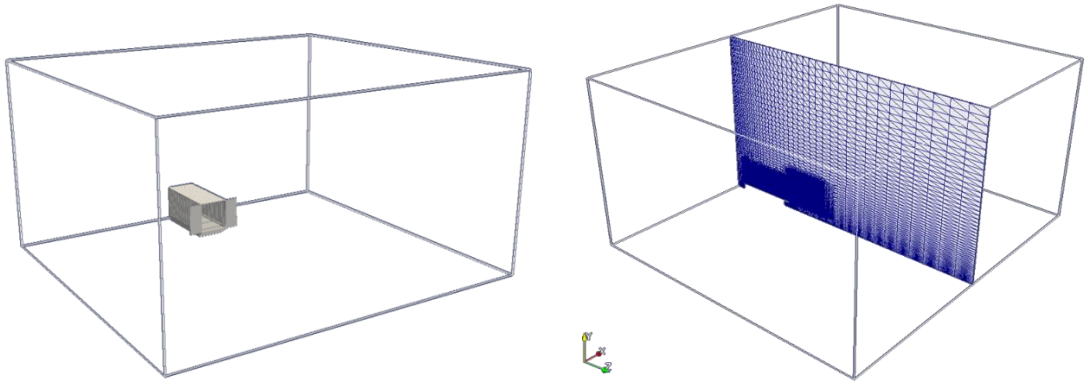

Figure 7. Computational domain and the mesh distribution in vertical cut plane

The container walls are assumed to be rigid. The boundary conditions applied to the geometry were non-slip, adiabatic walls for the chamber walls and ground. The 'totalPressure' and 'pressureInletOutletVelocity' boundary conditions were used for pressure and velocity respectively at the open boundaries. This combination of pressure and velocity boundary condition allows for the reverse flow at the open boundary patch. The mixture concentration of 15% volume hydrogen in air has approximately 0.42 equivalence ratio, the unstretched laminar flame speed is around 0.35 m/s, Lewis number is 0.42 and mixture fraction 0.0122, these values are used in the numerical simulations setup along with an ambient condition of 1 atm pressure and 298 K temperature with no wind conditions. An open vent was used in the simulations with premixed fuel mixture initialized in the chamber volume. The random velocity field of the turbulence root mean square velocity u'= 0.1 m/s was initialized in the entire domain.

5.0 RESULTS AND DISCUSSION

The numerical predictions along with the experimental measure value are plotted in Figure 8 for the case-1 scenario at P1 location i.e., empty container with steel frame at 15 % vol concentration of hydrogen. The overpressure trace curves obtained in the experiment at location P1 (P2) is only used in the present study to compare the numerical predictions, (at the moment only this experimental trace curve is available with the authors to publish). The numerical predicted pressure trace curve is moving time averaged for 5 ms to smoothen the curve and for getting the mean trends of the overpressure curves (similar to operating a low-pass filter, filtering the high frequency oscillations). Figures 8(a) and 8(b) are without and with time averaging of the pressure trace curves. It is discernable from Figure 8(b) that the time averaged pressure trace curves provide a better comparison to the experimental results, hence the remaining pressure-trace curves are also time averaged for 5 ms. the initial pressure rise was well captured in the numerical predictions.

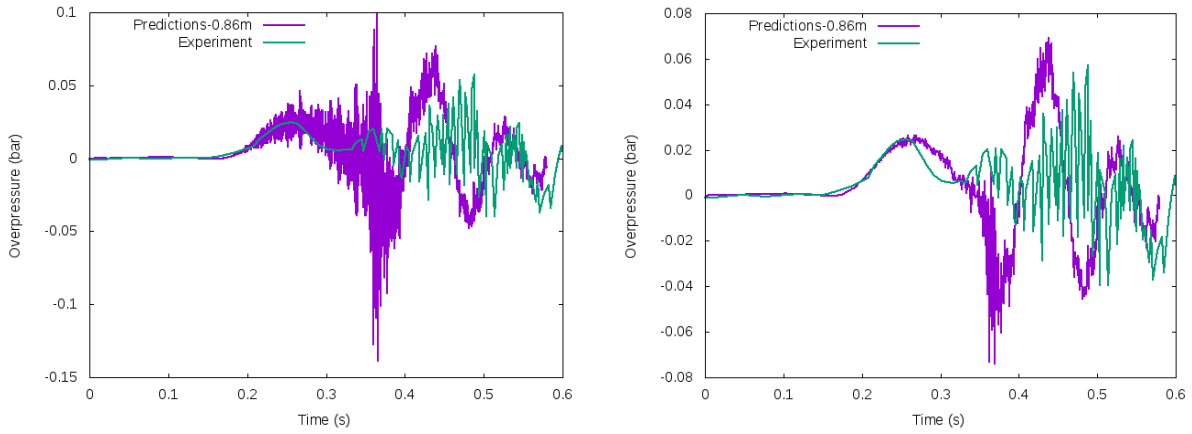

(a) Instantaneous pressure profile (b) Time averaged profile for 5 ms

Figure 8. Pressure trace curve for P1 pressure probe location (at 0.86 m) along with experiment measurements.

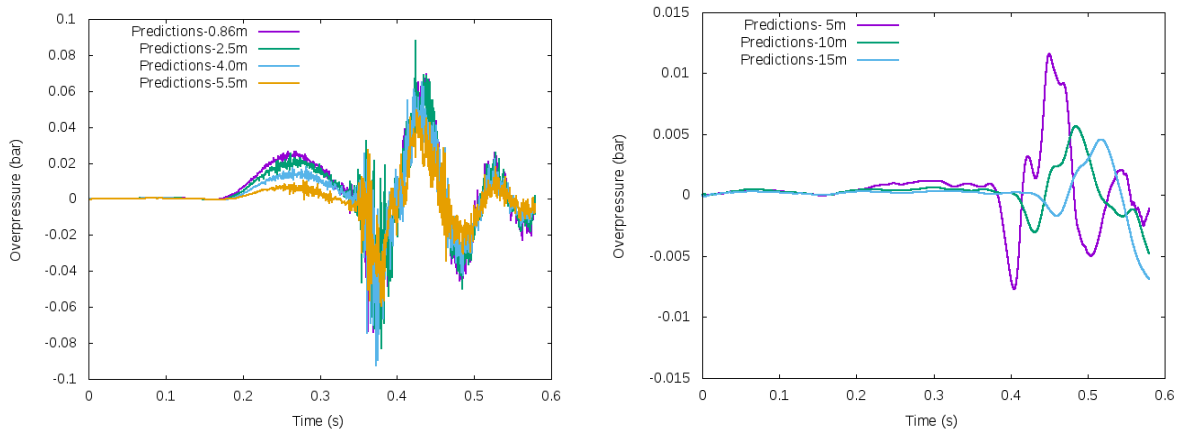

(a) Inside the container, (b) Outside and in front of the open container door

Figure 9. Numerical predicted of pressure trace curve for pressure probes (time averaged 5 ms).

The predicted overpressure trace curves for the pressure probe located within the container are shown in Figure 9(a) and outside in-front of the open container in Figure 9(b) after time averaging the curves for 5 ms. The peak pressure is case-1 scenario is obtained at P1 (P2) location. As the hot gas continue to expand through the open doors, the overpressures are reducing along the length of the container

(considering the first pressure peaks in the pressure trace curves). The second peak in the pressure trace curves in the container is much more oscillatory due to the presence of Helmholtz oscillation generated by venting of the bulk of the hot gases. The frequency of the oscillations observed in experiments also had the contributions from the structural vibrations of the container walls, which are not present in the numerical results due to treating the container wall as rigid in the numerical simulations, Therefore the numerical predictions are only commented based on the first peak pressure values observed in the individual trace curves. The numerical predictions shown in Figures 8 and 9 for empty container (with frame) will serve as base case to study the effect of the congestion/obstacles present within the container on the generated overpressures.

The Case-2 scenario results for the container with bottle basket as congestion placed near to the back wall are shown in Figure 10. The overpressures are higher in magnitude than that observed in the base case. The overpressure trends to increase initially and then reduced towards the end of the container. Clearly showing the influence of the bottle basket congestion on the flame propagation. The acceleration of the flame around the obstacles leads to generation of higher overpressures. The obstacles contributes in increasing the flame surface area due to flame stretch and straining around them thereby increasing flame consumption rate.

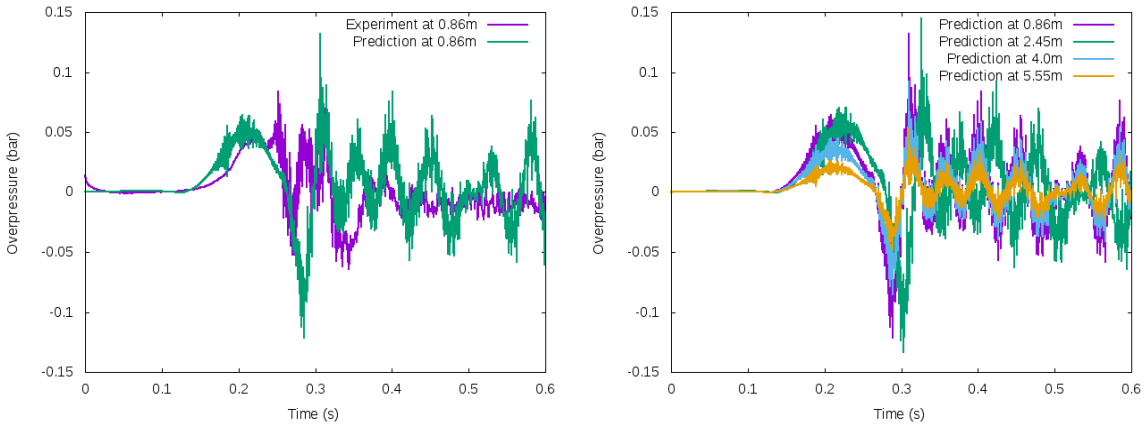

(a) Overpressure trace curve at P1 location (b) Time averaged profile inside the container

Figure 10. Pressure trace curve for P1 pressure probe location along with experiment measurements in case-2 scenario with bottle basket as obstacles.

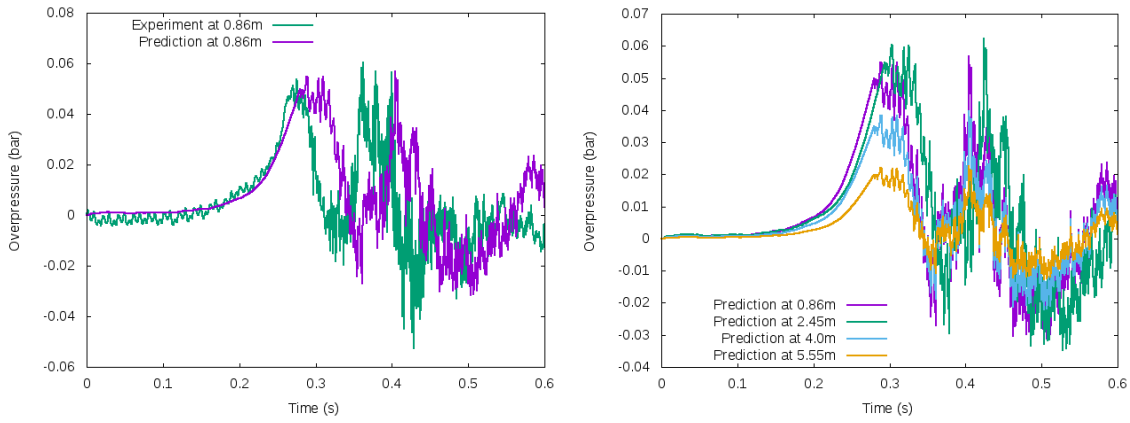

(a) Overpressure trace curve at P1 location (b) Time averaged profile inside the container

Figure 11. Pressure trace curve for P1 pressure probe location along with experiment measurements in case-3 scenario with pipe rack as obstacle.

Case-3 scenario which contains pipe rack as obstacles are shown in Figure 11. The overpressures measured in experiments and numerical simulation at P1 pressure probe are shown in Figure 11(a), the initial pressure rise and the first peak overpressure are well captured in the numerical predictions. The peak overpressure trends along the container shown in Figure 11 (b). The trend is similar to that observed in the case-2 scenario with the bottle basket as obstacles. There is initial increase in overpressure magnitude and then once the flame pass through the obstacle the peak overpressure values starts decreasing as the hot gases escape to the atmosphere. The bottle basket more over acts like a single large obstacles and the pipe rack acts more like a distributed and porous obstacle, still they both contributed to almost the same rise in overpressure. Although one can argue that the pipe rack should contribute for generation of higher overpressure due to possibility of creating larger flame surface area, the similar in trends of the overpressures in case-2 and case -3 could be due to the closer placement of obstacles to the ignition location and hence enough flame surface was not generated before actual interactions with the obstacles.

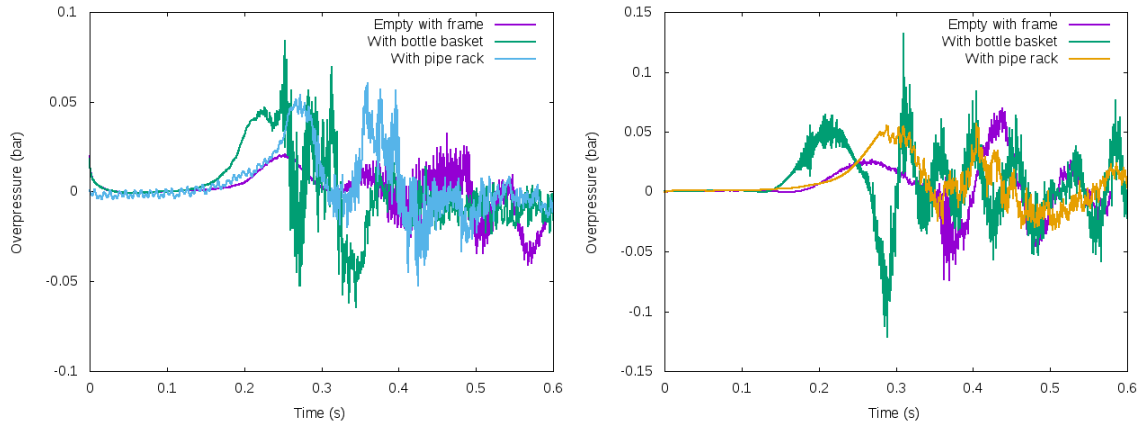

(a) Experiments results (b) Numerical predictions

Figure 12. Pressure trace curve for P1 pressure probe location (at 0.86 m) for three scenarios.

The overall trend of the overpressure at the P1 pressure probe location are shown in a single plot for experimental in 12 (a) and numerical predictions in 12 (b). Although the pressure trace curves locally vary in profile to that of the experiments but the overall trends in terms of the overpressure magnitudes are well captured in the numerical predictions. The peak overpressures at P1 location in case-2 and case-3 are almost twice higher than that observed in the base case-1 scenario. Clearly the constriction in the flow path of the flame contributed for the higher overpressures. The knowledge of these increase in overpressure values due to contributions of the different process equipment (obstacles) is very essential in designing and safely operating the new hydrogen installations, such as the portable self-contained power generation units.

6.0 CONCLUSION

The 20-ft ISO containers are being considered for developing self-contained portable power generation units using the fuel cell technologies. The possible scenarios of lean hydrogen-air deflagrations in these containers are being studied numerically in the present study. Experimental data from full scale container tests carried out by Gexcon (submitted separately for this conference), are used for model validation. The modification to flame speed correlation and turbulent flame speed considered in the present study result in reasonable accuracy of numerical predictions to experiments. The first overpressure peak is well predicted and with discernable time lags in occurrences of pressure peaks in the later parts of the pressure trace in numerical results, wherein the structural response trends to influence the generated overpressures. The container walls are modelled as rigid surface in the numerical modeling. The results have demonstrated the potential of the present numerical modelling for simulating lean hydrogen-air mixtures deflagrations in vented explosions scenarios in containers.

The overall effects of obstacles on the turbulent deflagration is qualitatively well captured in the numerical predictions. As observed in Figure 12, the vented explosion of 15 % vol concentration of hydrogen in the container with obstacles produced nearly twice the overpressures in magnitude to that of in the empty container. Such information is very vital in designing the process equipment and also defining the safety distances around the hydrogen process installations.

Acknowledgements

The HySEA project (www.hysea.eu) receives funding from the Fuel Cells and Hydrogen Joint Undertaking under grant agreement No 671461. This Joint Undertaking receives support from the European Union's Horizon 2020 research and innovation programme and United Kingdom, Italy, Belgium and Norway.

REFERENCES

1. Mccann, P. J., Thomas, G. O., Edwards, D. H. (1985) Geodynamics of Vented explosions Part I: Experimental studies, Combustion and Flame, 59 : 233-250.
2. Cooper, M. G., Fairweather, M., & Tite, J. P. (1986). On the mechanisms of pressure generation in vented explosions. Combustion and Flame, 65(1), 1-14.
3. Molkov, V.V., Baratov, A.N., and Korolchenko, A.Y., Dynamics of gas explosions in vented vessels: a critical review and progress, Progress in Astronautics and Aeronautics, 154: 117-131 (1993).
4. Bauwens, C. R., Chaffee, J., & Dorofeev, S. (2010). Effect of Ignition Location, Vent Size, and Obstacles on vented Explosion Overpressures in Propane-Air Mixtures. Combustion Science and Technology, 182(11), 1915 – 1932.
5. Bauwens, C.R., Chaffee, J., and Dorofeev, S.B., "Experimental and Numerical Study of Hydrogen-Air Deflagrations in a Vented Enclosure," in 7th ISHPMIE proceedings Vol. 1, St. Petersburg, Russia, 2008.
6. Molkov,V.V, R. Dobashi, M. Suzuki and T. Hirano, Modelling of Vented Hydrogen-Air Deflagrations and Correlations for Vent Sizing, *J. Loss Prev. Process*, **12**, 1999, pp. 147-156.
7. Bauwens, C.R., Chaffee, J., and Dorofeev, S.B., "Vented Explosion Overpressures from Combustion of Hydrogen and Hydrocarbon Mixtures," IJHE, vol. 36, no. 3, pp. 2329–2336, Feb. 2011.
8. Bauwens, C. R, Dorofeev, S. B, Effect of initial turbulence on vented explosion overpressures from lean hydrogen air deflagrations, Int. Journal of Hyd. Energy, 39, 2014.
9. Abdel-Gayed R. G., Bradley, D, Hamid M., N. Lawes, M., Lewis number effects on turbulent burning velocity (1985), Twentieth Sym. on Combust.
10. Chakarborty, N., Cant, R.S, Effects of Lewis number on flame surface density transport in turbulent premixed combustion (2011). Comb. and Flame. 9:158.
11. www.openfoam.org.
12. Fureby, C., et al., A comparative study of subgrid scale models in homogeneous isotropic turbulence. Physics of Fluids, 1997. **9**(5): p. 1416-1429.
13. Weller, H. G., Tabor, G., Gosman, A. D., and Fureby, C., Application of a flame wrinkling LES combustion model to a turbulent mixing layer (1998), Proc. of Combust. Inst., 27.
14. Tabor, G. and H.G. Weller, Large Eddy Simulation of Premixed Turbulent Combustion Using Ξ Flame Surface Wrinkling Model. Flow, Turbulence and Combustion, 2004. **72**(1): p. 1-27.
15. Muppala Reddy, S. P., Aluri Naresh K., Dinkelacker, F., Development of an algebraic reaction rate closure for the numerical calculation of turbulent premixed methane, ethylene, and propane/air flames for pressure up to 1.0 MPa (2005), Combust. And Flame, 140.
16. Burke, E., M., Singlitico A., Morones, A., Petersen, E., L., Guthe, F., BiruteBunkute, Speth, R., L., Monaghan, R., F., D., progress towards a validated Cantera-based turbulent flame speed solver (2015), Proc. of the European Combust. Meeting.

17. Muppala, S., P., R., Nakahara, M., Aluri, H., Kido, Wen, J. X, Papalexandris, M. V., Experimental and analytical investigation of the turbulent burning velocity of two-component fuel mixtures of hydrogen methane and propane (2009), Int. Journal of Hyd. Energy, 22:34.
18. Goulier, J. Comandini, A., Halter, F., Chayumeix, N., experimental study on turbulent expanding flames of lean hydrogen/air mixtures (2016), Proc. Combust. Inst.
19. Kitagawa, T., Nakahara, T., Maruyama, K, Kado, K., Hayakawa, A., Kobayashi, S., Turbulent burning velocity of hydrogen-air premixed propagating flames at elevated pressure (2008), Int. Jol. of hyd. Energy, 20:33.
20. Verhelst, S., A laminar velocity correlation for hydrogen/air mixtures at spark ignition engine conditions (2003), Spring Technical Conf. of ASME internal Combust. Engine division, ICE2003.
21. www.hysea.eu, HySEA first blind predictions study, " Hydrogen explosion in ISO containers with homogenous mixtures". Doc. no.: HySEA-D-4-05-2016.